INFLUENCE OF THE PLASMA EDGE ON TOKAMAK PERFORMANCE

H R Wilson, J W Connor, A R Field, S J Fielding, R J Hastie, R L Miller[1] and J B Taylor
EURATOM/UKAEA Fusion Association,
Culham Science Centre,
Abingdon, Oxon OX14 3DB
UK

Abstract
A number of edge plasma physics phenomena are considered to determine tokamak performance: transport barrier, edge magneto-hydrodynamic (MHD) instabilities, plasma flow. These phenomena are thought to be causally related: a spontaneous increase in the plasma flow (actually, its radial variation) suppresses heat and particle fluxes at the plasma edge, to form a transport barrier; the edge pressure gradient steepens until limited by MHD instabilities, resulting in a temperature pedestal at the top of the steep gradient region; a number of core transport models predict enhanced confinement for higher values of the temperature pedestal. This paper examines these phenomena and their interaction.

1. INTRODUCTION

The H-mode is the most developed mode of high confinement tokamak operation. Fundamental to its success is the transport barrier which is formed close to the plasma edge; this paper is concerned with the physics of this barrier. We describe MHD instabilities associated with the steep pressure gradient region: in particular the peeling mode, driven by current density, and the ballooning mode, driven by pressure gradient. This suggests a model for edge localised instabilities (ELMs) and an explanation for the difficulty experienced in achieving H-mode in low density COMPASS-D discharges. We then apply the analytic ballooning theory techniques developed for this MHD study to analyse edge drift mode structures, and show that these can, in principle, drive a plasma flow over a region $\sim\rho_*^{2/3}a$, where ρ_* is the ion Larmor radius, normalised to the plasma minor radius a. Combining this with the assumption that the flow suppresses the plasma turbulence we obtain an expression for the transport barrier width which, together with the limit set on the pressure gradient by the MHD instabilities, leads to a prediction for the temperature pedestal. We close with a discussion of future work.

2. EDGE LOCALISED INSTABILITIES

Two edge-localised instabilities are discussed in the literature: the peeling mode, driven by edge current density [1] and the ballooning mode driven by pressure gradient [2]. The peeling mode is highly localised at the plasma surface, while the ballooning mode spans many rational surfaces and, as we shall see, can be relatively extended. We first review each of these instabilities in turn.
The peeling mode has been addressed assuming a limiter geometry, when it is found to be most dangerous when there is a rational surface just outside the plasma. In this case, the stabilising influence of magnetic perturbations in the vacuum can be neglected and a necessary stability criterion for the mode is [3]:

$$\sqrt{1-4D_M} > 1 + \frac{1}{2\pi q'}\oint \frac{J_{\|}B}{R^2 B_p^3}\,dl \qquad (1)$$

where D_M is the Mercier coefficient; $D_M<1/4$ is the Mercier criterion for stability. We have defined $J_{\|}$ as the current density parallel to the magnetic field B, B_p is the poloidal field, R is the major radius, dl is the poloidal arc length element, q is the safety factor and a prime denotes differentiation with respect to the poloidal flux, ψ; all quantities are evaluated at the plasma surface. Recalling that D_M is proportional to the pressure gradient, Eq (1) demonstrates that this instability is driven by current density, and stabilised by pressure gradient.
The ballooning mode theory was originally developed for high toroidal mode number n, pressure-driven instabilities in the core and, in the limit that the toroidal mode number $n\to\infty$, stability is determined by an ordinary differential equation along the magnetic field line: the ballooning equation [2]. This provides a value for a 'local' mode frequency as an eigenvalue which is a function of the poloidal flux, ie $\omega^2(\psi)$. Of course in practice n is not infinite, and then the mode has a finite radial extent. A consistent ordering is developed making use of the different radial

[1] General Atomics San Diego CA 92186-5608 USA

length scales associated with the equilibrium variation, characterised by $\omega^2(\psi)$, and the distance between mode rational surfaces, $1/nq'$. In the region where $\psi=\psi_0$, with $\partial\omega^2/\partial\psi|_{\psi=\psi 0}=0$ (ie the most unstable region, and therefore the one of interest), the mode is localised, spanning $\sim n^{1/2}$ rational surfaces. This permits the radial mode structure to be evaluated by developing an expansion in powers of $n^{-1/2}$, resulting in a Gaussian radial mode structure and an expression for the true mode frequency, $\Omega^2= \omega^2(\psi_0)+O(n^{-1})$, where the finite n corrections are stabilising. Thus the ballooning mode properties can be obtained from the leading order ballooning equation, without the need to address the higher order theory. However, the applicability of the leading order equation relies on the existence of the higher order theory.

Here we are interested in analysing ballooning mode stability at the plasma edge, in the vicinity of the H-mode transport barrier. Indeed, this is often the most interesting place to investigate ballooning modes because this region will have the steepest pressure gradient. In such situations $\partial\omega^2/\partial\psi$ will not be zero in general and the conventional higher order ballooning theory is invalid; a new ballooning theory has been developed for this situation. In Section 4 we shall illustrate an application of this theory to study edge drift-ballooning modes; the application to ideal MHD ballooning modes is covered elsewhere in the literature [3], so here we simply state the results of this modified theory. Following an expansion in $n^{-1/3}$, the key results are:

- the leading order ballooning equation is identical to the conventional ballooning equation, which can be used to derive $\omega^2(\psi,k)$, where k is the ballooning phase angle;
- as with conventional ballooning theory, k is chosen to maximise the instability;
- the radial mode structure is the tail of an Airy function, spanning $\sim n^{1/3}$ rational surfaces;
- the true mode frequency is related to the local value by $\Omega^2= \omega^2(\psi_0)+O(n^{-2/3})$

Thus, to leading order the conventional ballooning theory *can* be used to estimate ballooning stability at the plasma edge, although the radial mode structure and finite n corrections are different.

Ballooning stability is usually expressed in terms of the s–α diagram where, for a large aspect ratio, circular cross section equilibrium

$$\alpha = -\frac{2\mu_0 R q^2}{B^2}\frac{dp}{dr} \qquad s = \frac{r}{q}\frac{dq}{dr} = 2\left(1-\frac{J_\parallel}{\langle J_\parallel\rangle}\right) \tag{2}$$

Here r is the minor radius and p is the plasma pressure. For this equilibrium, the shear is related to the plasma current density, $J_\parallel$, as shown in Eq (2), where $\langle J_\parallel\rangle$ is the average current density (ie plasma current divided by cross-section area). Using this relation we can combine the ballooning and peeling mode stability criteria on a single diagram as shown schematically in Fig 1.

Figure 1 provides a picture of both the density threshold for the L-H transition observed in COMPASS-D [4] and ELMs. Thus, in a large aspect ratio, shifted circle equilibrium, the peeling mode criterion [Eq (1)] can be written in the form:

$$\alpha\left(\frac{r}{R}\left(1-\frac{1}{q^2}\right)+s\Delta' - f_t\frac{Rs}{2r}\right) > Rqs\left(\frac{J_\parallel^{\text{driven}}}{B}\right)_{\text{edge}} \tag{3}$$

Here Δ' is the radial derivative of the Shafranov shift, and this contribution arises due to the Pfirsch-Schlüter part of the parallel current (note this is stabilising) and f_t is the trapped particle fraction; the destabilising bootstrap current term is that proportional to f_t, while the Mercier coefficient reduces to the first term on the left-hand side. Only the driven current (eg Ohmic) appears on the right-hand side of Eq (3). In the banana collisionality regime $f_t\sim\sqrt{\varepsilon}$ and the bootstrap current term dominates the left hand side so that the peeling mode is always unstable.

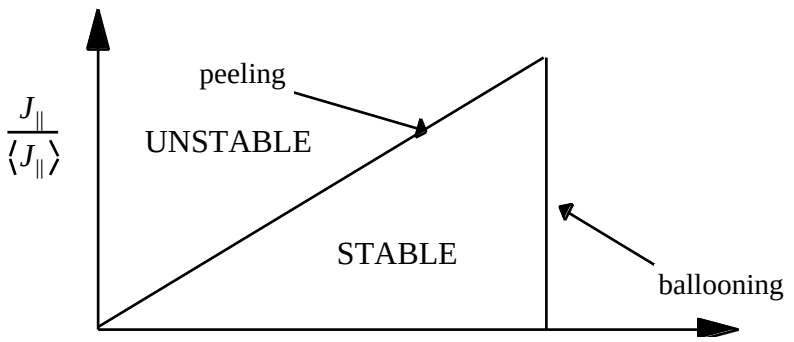

Figure 1: Schematic stability diagram for peeling and ballooning modes

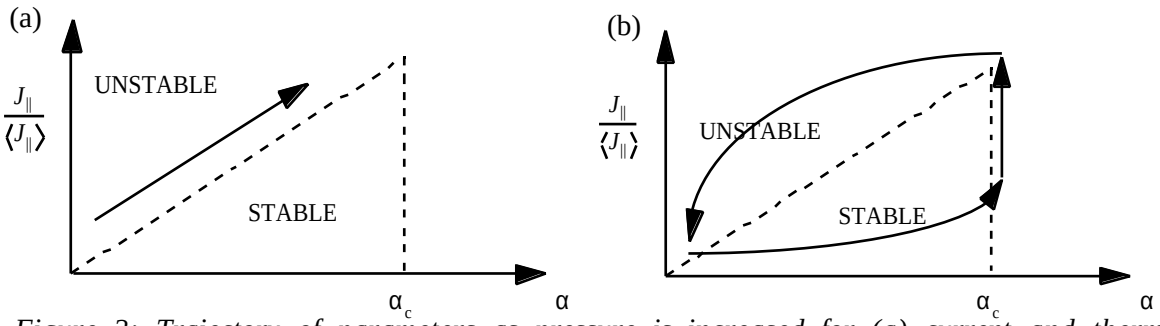

Figure 2: Trajectory of parameters as pressure is increased for (a) current and thermal diffusion time-scales comparable and (b) long current diffusion time-scales compared to thermal diffusion.

At higher collisionality $f_t \rightarrow 0$ and then the peeling mode can be stabilised by raising α, eg by increasing the heating power. If one adopts the assumption that it is necessary to stabilise the peeling mode in order to make a transition from L to H-mode, then this simple picture suggests that it is not possible to enter the H-mode at low collisionality. This provides an explanation of the density threshold observed on COMPASS-D: if the density is sufficiently low that the collisionality $\nu_* < 1$, then the bootstrap current is large and the trajectory on the stability diagram is as in Fig2a, so that the peeling mode cannot be stabilised. However, at higher density, the bootstrap current contribution is weakened, and the peeling mode can be stabilised at sufficiently high α (or heating power). Data on α versus ν_* from COMPASS-D is shown in Fig 3, demonstrating that the H-mode does indeed correspond to the high α, high ν_* region, with ELMs close to the 'stability' boundary, and L-mode at either low α or low ν_*. Note that the region at high α, low ν_* cannot be accessed because the L-mode confinement is too low to achieve significant edge pressure gradients with the heating power available. For larger tokamaks, where the current diffusion time is long compared to the thermal diffusivity, one might expect a trajectory more like that in Fig 2b. Thus, while α may rise relatively fast up to the ballooning limit, the current takes longer to reach its steady state value, consistent with the rise in α. One would then expect the transport from the ballooning mode to prevent α from rising beyond α_c, while the current slowly increases to its steady state value. When the current rises so that the plasma reaches the top corner of the stable 'triangle' it must enter the unstable region. The resulting plasma turbulence would then be expected to reduce the pressure gradient, further enhancing the instability and leading to a crash event; we interpret this as a Type I ELM.

The ability of this model to qualitatively explain some of the experimental observations motivates the development of a more quantitative model, allowing for the coupling of the ballooning and peeling modes. The coupled mode structure and stability must be derived by solving the full 2-D system of equations; we describe this procedure in the following section.

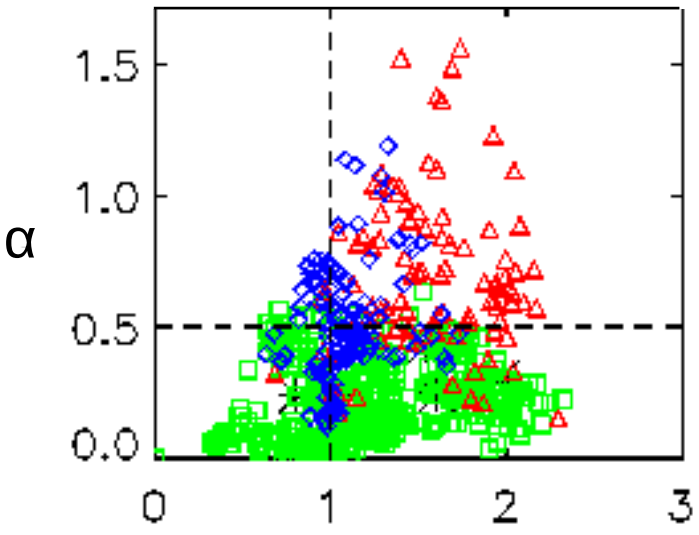

Figure 3: Data from COMPASS-D showing the distribution of L-mode and H-mode discharges. The measurements were taken with the HELIOS diagnostic, which uses optical spectroscopy from a thermal helium beam [5].
Symbols represent:

□: *L mode*

Δ: *H-mode with no ELM occurring during the measurement*

◊: *H-mode with an ELM occurring during the measurement*

3. COUPLED PEELING-BALLOONING MODES

To illustrate the essential features of the coupled peeling-ballooning mode structure and stability, we restrict consideration to the large aspect ratio, circular cross section equilibrium model. At high n the perturbed energy can be expressed in terms of the radial component of displacement, X, which we Fourier transform in poloidal angle:

$$X = e^{-im_0\theta} \sum_m u_m(x)\, e^{im\theta} \tag{4}$$

where $x=m_0-nq$, m_0 is the poloidal mode number associated with the vacuum rational surface closest to the plasma and θ is the poloidal angle. The Euler equations minimising the plasma energy then become a set of ordinary, coupled differential equations to be solved for the $u_m(x)$:

$$s^2 \frac{d}{dx}\left[(x-m)^2 \frac{du_m}{dx}\right] - (x-m)^2 u_m + \alpha d_M u_m = \alpha A_{m,m'} u_{m'} \tag{5}$$

where $A_{m,m'}$ involves first order differential operators in x and a sum over m' is implied. A magnetic well has been introduced through the parameter d_M where $D_M=\alpha d_M/s^2$, and α decreases linearly with radius from the edge. Boundary conditions on these equations are that each of the $u_m \to 0$ as $x \to \infty$ and that at the plasma-vacuum interface ($x=\Delta$) they must satisfy

$$(\Delta-m)\left[-s(\Delta-m)\frac{du_m}{dx} - \left[2-(\Delta-m)\right]u_m + \frac{\alpha}{2}(\Delta-m)\left(u_{m+1}-u_{m-1}\right)\right]_{x=\Delta} = \Omega^2 u_m \tag{6}$$

where Ω^2 is an eigenvalue such that $\Omega^2<0$ corresponds to instability (we are interested in marginal stability here), and m is a shifted poloidal mode number. The effect of the vacuum energy has been included in Eq (6) and we have replaced the current density with magnetic shear, s.

From the system of Eqs (5) and (6) one can analytically derive the equations describing both ballooning and peeling modes. First, employing a local expansion about the single vacuum rational surface labelled m_0 and taking $\Delta<<1$ gives the peeling mode criterion:

$$\alpha > \frac{2(2-s)}{-d_M} \tag{7}$$

for stability. Employing the 'ballooning approximation' for more radially extended modes, $u_m(x)=e^{imk}u(x-m)$, we derive the familiar s–α equation, modified for the effect of the magnetic well [6]. The stability diagram of the coupled peeling-ballooning mode (Fig 4) retains some of the features of these stability boundaries, but depends on the value of Δ, (for $\Delta\approx 1$ the stabilising influence of the vacuum suppresses the peeling mode). We see that for small Δ the marginal stability boundary approximately follows the peeling and ballooning mode boundaries, while for larger Δ the peeling mode plays no role, and only the ballooning mode boundary matters.

It is interesting to consider how the s–α stability diagram is modified. In particular we are interested in access to the second stability regime, which is usually gained at low magnetic shear. However, the peeling mode is unstable at low magnetic shear (see Eq (7)) so it is necessary to

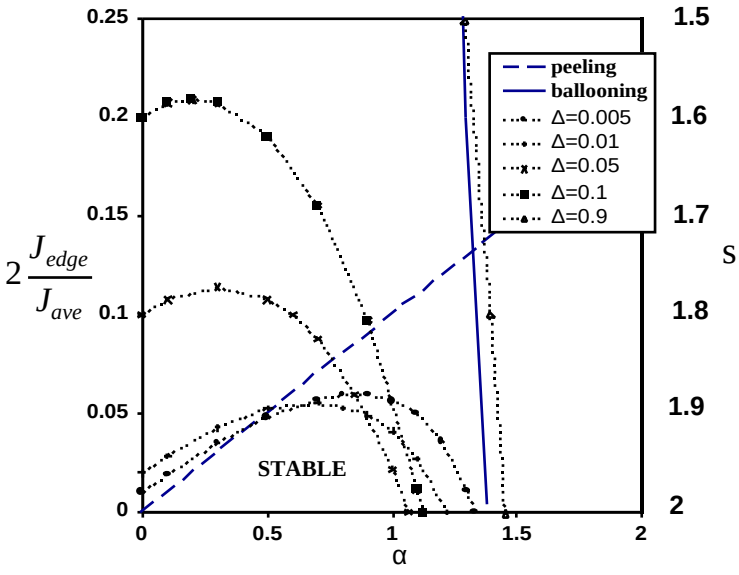

Figure 4: Marginal stability contours for the coupled peeling-ballooning mode system for a number of different Δ (dotted curves) compared with the pure ballooning mode (full curve) and pure peeling mode (dashed curve) stability boundaries. Parameters are $d_M=-0.2$, $q=4$, $n=10$.

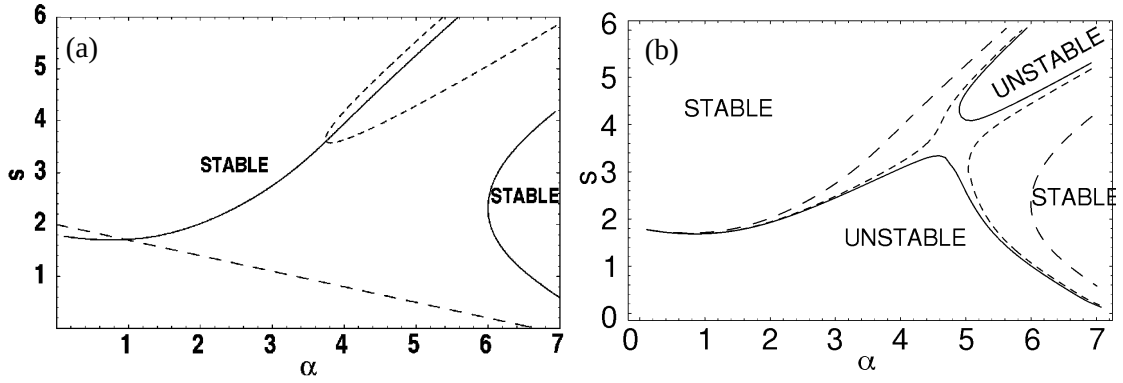

Figure 5: Marginal stability contours in the s–α plane for (a) ideal n=∞ ballooning (dotted), peeling (dashed) and coupled peeling-ballooning (full) modes (d_M=-0.6) and (b) coupled modes for d_M=-0.6 (dashed), d_M=-0.64 (dotted) and d_M=-0.645 (full). Here Δ=0.1, q=4, n=20.

revisit second stability at the plasma edge. Choosing a high value for the magnetic well parameter, d_M=-0.6, we show in Fig 5a the individual peeling (dashed) and ballooning (dotted) stability boundaries which indicate that although the window to second stability is reduced in size, it still remains. However, when one calculates the stability of the *coupled* mode for the same parameters, one finds that the effect of the coupling is to remove the stable window and so prevent second stability access (full curves). In order to regain access to second stability it is necessary to increase the depth of the magnetic well still further, as shown in Fig 5b. Thus increasing d_M=-0.64 one sees a 'necking' of the unstable region, which then breaks to give second stability access at d_M=-0.645; further increases in the well depth leads to a separation of the peeling and ballooning mode boundaries and improved second stability access.

We now consider the radial mode structure. Figure 6a shows a typical peeling mode structure, which is dominated by the Fourier harmonic associated with the vacuum rational surface closest to the plasma surface, but with several sideband harmonics which couple because of the toroidal geometry. Figure 6b shows the ballooning mode structure. Two things are apparent from the ballooning mode structure: there are many more harmonics involved than for the peeling mode, and the amplitude is peaked away from the plasma edge. Indeed, the amplitude is fitted well by taking the Airy function envelope which arises from the approximate analytic theory [3], as shown by the dashed curve in Fig 6b. This ballooning mode penetrates a large distance ~0.05*a* into the plasma, comparable to the H-mode barrier width.

4. EDGE DRIFT-BALLOONING MODES AND REYNOLDS STRESS

The drift mode equation provides an interesting application of the edge ballooning theory mentioned in Section 2. This equation, which encompasses both the ion-temperature-gradient (ITG) mode and electron drift wave, can be simplified in a large aspect ratio, circular flux surface tokamak geometry [7]:

$$\left[\frac{1}{(nq')^2}\frac{\partial^2}{\partial y^2} - \frac{\sigma^2}{\Omega^2}\left(\frac{\partial}{\partial\theta} - inq'y\right)^2 - \frac{\alpha}{\Omega}\left(\cos\theta - \frac{is}{nq'}\sin\theta\frac{\partial}{\partial y}\right) - \Lambda\right]\varphi = 0 \qquad (8)$$

where φ is the perturbed electrostatic potential, the radial coordinate $y=r_0-r$ where r is the minor

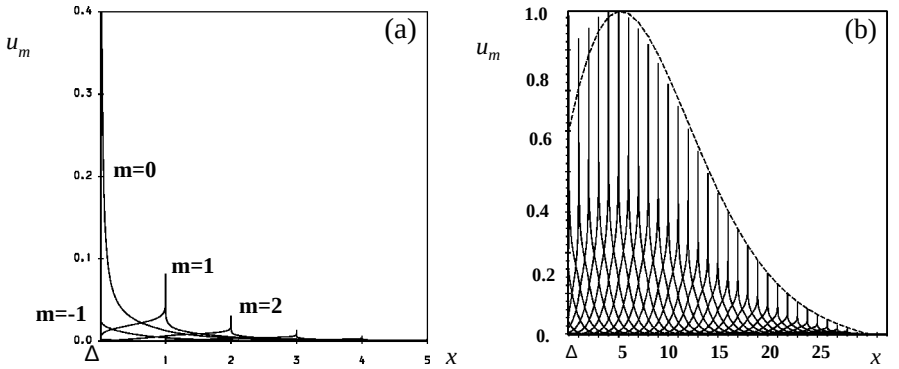

Figure 6: Radial mode structure for (a) peeling mode (Δ=0.01, n=10, α=1.0, s=1.945) and (b) ballooning mode (Δ=0.9, n=40, α=1.41, s=2.0).

radius and r_0 the reference rational surface, which we choose to be the last one in the plasma, θ is the poloidal angle and a prime denotes a radial derivative. Other parameters of the model are $\alpha=2\varepsilon/bs^2$, $\sigma=\varepsilon/bqs$, $\varepsilon=L_n/R\tau$, $\tau=T_e/T_i$, $b=(k_\theta\rho_i)^2/2$, $\Omega=\omega/\omega_{*e}$, and

$$\Lambda = \frac{1}{bs^2}\left[\frac{\Omega-1}{1+\tau+\eta_i} - b\right] \tag{9}$$

where L_n is the density gradient length scale, η_i is the ratio of density to ion temperature length scale, T_j is the temperature of the species j, k_θ is the poloidal wave number, ρ_i is the ion Larmor radius, ω is the complex mode frequency and ω_{*e} is the electron diamagnetic frequency. We first use the ballooning transform to write φ in the form:

$$\varphi = \sum_m e^{im\theta}\int_{-\infty}^{\infty} d\eta\; e^{-im_0(\theta-\eta)} e^{-im\eta} F(y,\eta)\exp\left[inq'(y\eta - S(y))\right] \tag{10}$$

and develop the solution to Eq (8) by defining an extended radial variable $z=n^{2/3}y$, anticipating $\partial F/\partial z=O(1)$ and expanding in $n^{-1/3}$:

$$\left(L_0 + n^{-1/3}L_1 + n^{-2/3}L_2 + \quad\right) + (\lambda + \Lambda)\left[F_0 + n^{-1/3}F_1 + n^{-2/3}F_2 + \quad\right] = 0 \tag{11}$$

where

$$\begin{aligned} L_0 &= \frac{\sigma^2}{\Omega^2}\frac{d^2}{d\eta^2} + (\eta-k)^2 + \frac{\alpha}{\Omega}\left[\cos\eta + s(\eta-k)\sin\eta\right] \\ L_1 &= \frac{i}{q'}\frac{\partial L_0}{\partial k}\frac{\partial}{\partial z} \qquad\qquad L_2 = -\frac{1}{q'^2}\frac{\partial^2}{\partial z^2} \end{aligned} \tag{12}$$

with $k=dS/dy$ and we assume $\Lambda-\lambda=O(n^{-2/3})$, which will be confirmed later. Thus to leading order $F_0=A(z)f_0(\eta)$ where

$$(L_0 + \lambda)\, f_0 = 0 \tag{13}$$

determines the ballooning eigenfunction f_0 and the 'local' eigenvalue $\lambda(r,k)$ (applying suitable boundary conditions in the limit $\eta\to\infty$, ie outgoing wave or bounded). The solubility condition on the $O(n^{-1/3})$ equation determines k through the condition

$$\frac{\partial\lambda}{\partial k} = 0 \tag{14}$$

which is the same condition as for a conventional drift-ballooning mode. As with the MHD ballooning mode, the difference arises in the radial mode structure, where the envelope satisfies

$$\frac{1}{2q'^2}\frac{\partial^2\lambda}{\partial k^2}\frac{d^2A}{dz^2} + n^{2/3}(\Lambda-\lambda)A = 0 \tag{15}$$

Taylor expanding λ about the edge, it has an essentially linear radial dependence, and therefore Eq (15) is again an Airy equation for the envelope function $A(z)$.

To illustrate the essential features of drift-ballooning modes we simplify the problem to consider the slab branch of the η_i mode in the limits $\sigma/\Omega<<1$, $\alpha/\Omega<<1$ and $\eta_i>>1$. This allows us to expand the trignometric functions about $\eta=k$, to deduce:

$$\lambda = \mp\frac{i\sigma}{\Omega} - \frac{\alpha}{\Omega}\cos k \qquad f_0 = \exp\left[\pm\frac{ia}{2}\left(\eta - k + \frac{c}{2a^2}\right)^2\right] \tag{16}$$

where

$$a^2 = \frac{\Omega^2}{\sigma^2}\left[1 + \frac{\alpha}{2\Omega}(2s-1)\cos k\right] \qquad c = \frac{\alpha\Omega}{\sigma^2}(s-1)\sin k \tag{17}$$

Using Eq (14), we choose $k=0$, and the dispersion relation $\lambda\approx\Lambda$ determines Ω, so that we have:

$$\Omega = -(1-i)\sqrt{\frac{\varepsilon s\eta_i}{2q}}\left[1 - \frac{2iq}{s}\right]^{1/2} \qquad f_0 = \exp\left[-\frac{(1+i)}{2}bs\sqrt{\frac{sq\eta_i}{2\varepsilon}}\left[1-\frac{2iq}{s}\right]^{1/2}\eta^2\right] \tag{18}$$

Having determined the radial mode structure we can now calculate the Reynolds stress [8]:

$$R_y = \frac{1}{r}\left\langle\frac{\partial\varphi}{\partial\theta}\frac{\partial\varphi}{\partial r} + \frac{\partial\varphi}{\partial\theta}\frac{\partial\varphi}{\partial r}\right\rangle \tag{19}$$

where angled brackets denote an average over the poloidal angle and a star denotes complex conjugate. It is convenient to calculate this in real space rather than ballooning space, and we therefore write

$$\varphi = \sum_{m=0}^{\infty} e^{-im_0\theta} e^{im\theta} A_m u_m(x) \tag{20}$$

where $m_0=nq(r_0)$, A_m is the Airy envelope solution to Eq (15) evaluated at the rational surface labelled by shifted poloidal mode number m and $u_m(z)$ is related to the solution of the ballooning equation:

$$u_m(x) = C\int_{-\infty}^{\infty} d\eta\, f_0(\eta) e^{i\eta(x-m)} = \exp\left[-(1-i)\mu^2(x-m)^2\right] \tag{21}$$

Here $x=nq'(r_0-r)$, C is a normalisation factor and for the ITG branch $\mu^2=(1/(4bs))\sqrt{(2\varepsilon/(sq\eta_i))}$ (we have taken $s>>q$ to simplify the expression for μ^2; this could represent a feature of separatrix geometry). The Reynolds stress can be reduced to the form

$$R_y = -\frac{2nq'}{r} m_0 \sum_{m=0}^{\infty} |A_m|^2 \,\mathrm{Im}\left(\frac{du_m}{dx} u_m^*\right) \tag{22}$$

which for the ITG mode branch becomes

$$R_y = -\frac{4nq'}{r} m_0 \sum_{m=0}^{\infty} |A_m|^2 \mu^2(x-m)\exp\left[-2\mu^2(x-m)^2\right] \tag{23}$$

For the strong ballooning limit which we considered above, we have $\mu<<1$ so that the sum over m can be replaced by an integral. This can be manipulated into the form

$$R_y = \frac{nq'}{r} m_0 \int_0^{\infty} dm \,\frac{d}{dm}|A_m|^2 \exp\left[-2\mu^2(x-m)^2\right] \tag{24}$$

Making use of the slow variation of $A(m)$ relative to the exponential factor, and neglecting an error function contribution (which is localised at the plasma edge where $|A|^2$ is small), we derive

$$R_y \sim \frac{m_0}{r^2} n^{2/3} |A|^2 \sqrt{\frac{\pi}{8\mu^2}} \tag{25}$$

This is our final result for the Reynolds stress. Note that we only include the contribution from a single n, assumed to dominate the spectrum. We have also neglected the contributions from the tails of 'core' drift modes, which are more stable (note λ is averaged over k for these modes, rather than choosing k to maximise the growth rate as is done for the edge drift modes).

The Reynolds stress provides a poloidal torque which spins the plasma; the magnitude of the flow depends on a balance between this torque and damping mechanisms such as neoclassical magnetic pumping or the effect of neutral particles, for example. Clearly the Reynolds stress depends on the amplitude $|A|^2$, which can only be determined by considering a non-linear saturation mechanism. This is beyond the scope of this work and therefore we do not address the magnitude of the flow, but assume it is sufficiently large to suppress turbulent diffusion. Equation (25) then suggests that a transport barrier will form over the radial extent of the linear mode,

$$\Delta r = L\left(\frac{q^2\rho^2}{4b}\right)^{1/3} \tag{26}$$

where $L=(\lambda_{kk}/(q'^2\lambda_x))^{1/3}$ is a typical equilibrium length scale, $L\sim r$. Combining this result with the result from the previous section, that the pressure gradient is tied to a value $\alpha=\alpha_c$ by the MHD ballooning mode, then we obtain an expression for the temperature pedestal, scaling as $\rho^{2/3}$:

$$T = \frac{B^2\alpha_c}{2\mu_0 Rq^2 n_e} L\left(\frac{q^2\rho^2}{4b}\right)^{1/3} \tag{27}$$

Of course the dependence of the temperature pedestal on the equilibrium parameters is model-dependent, and the model we have described here is rather simplistic. However, a robust feature of all edge drift-ballooning modes is the relation $\Delta r \sim \rho^{2/3} r$ and therefore, assuming the pressure gradient rises to the MHD ballooning limit, the temperature pedestal scaling as $\rho^{2/3}$ is also robust.

5. EFFECT OF FLOW ON MHD

To complete the 'loop' and develop a fully self-consistent model of the transport barrier it is necessary to address the effect of flow on the edge MHD instabilities discussed here. A number of features associated with the effect of sheared toroidal flow on the ballooning mode have been addressed. The introduction of plasma flow destroys the ballooning symmetry and the eigenmode problem is two-dimensional. Two approaches have been adopted in the literature: a conventional eigenmode approach, where the two dimensions are poloidal angle and radius, and a Floquet approach, where the two dimensions are time and ballooning coordinate. These yield the same long-time exponential growth, but the Floquet mode has an additional periodic time dependence [9,10]. This periodic time dependence is arbitrary when the sheared flow has a purely linear variation with radius; this arbitrariness is associated with the initial conditions. Introduction of a small quadratic radial variation of the flow results in a damping of the oscillations, so that after a time $\sim n$ Floquet periods the Floquet mode is identical to the eigenmode (note, the eigenmode can be considered as a particular Floquet mode, whose periodic time dependence is simply constant). Thus, the Floquet and eigenmode approaches are essentially equivalent. In the case with small flow, where it is possible to reduce the eigenmode system to a 1-D problem and evaluate the eigenvalue ω^2 as a function of the ballooning phase angle, k, one generally finds that part of the region $0 \le k \le 2\pi$ is stable, and part is unstable. For small shear flow one finds that the growth rate is obtained by averaging ω^2 over the unstable region of k, and the stable region plays no role. For larger flow, coupling to the stable continuum of ideal MHD results in an increased stabilisation due to a form of 'continuum damping', such that the growth rate falls approximately linearly with increasing flow shear; this surprising result has also been seen in numerical calculations [10].

6. DISCUSSION

We have provided an interpretation of ELMs in terms of well-known MHD instabilities, with an improved formalism to calculate their stability at the plasma edge. The edge pressure gradient is limited by the ideal MHD ballooning mode, and the ELMs are interpreted as a consequence of the edge current density (ie the boostrap and Ohmic currents), which drives the peeling mode; this could also explain the density threshold for L-H transitions in COMPASS-D. Future work will quantify the results of this model by including realistic geometry in the stability analyses, and development of a transport model to investigate the interactions between the different time-scales. The formation of the transport barrier is assumed to be a consequence of flow shear generation at the plasma edge, and a possible mechanism, arising from the Reynolds stress associated with drift-ballooning modes whose structure is modified close to the plasma edge, has been proposed. The result of this model is that the temperature pedestal scales as $\rho_*^{2/3}$; it is interesting to note that this is consistent with measurements made on the JET tokamak [11].

Acknowledgement: This work was supported by the UK Department of Trade and Industry and Euratom, and by the US Department of Energy under grant DE-FG03-95ER54309.

REFERENCES

[1] D Lortz, Nucl Fusion **15** (1975) 49
[2] J W Connor, R J Hastie and J B Taylor, Proc Roy Soc London A **365** (1979) 1
[3] J W Connor, R J Hastie, H R Wilson and R L Miller, Phys Plasmas **5** (1998) 2687
[4] S J Fielding et al, Plas Phys Contr Fusion **38** (1996) 1091
[5] A R Field, P G Carolan, N J Conway, M G O'Mullane, to appear in Rev Sci Instr **70** (1999)
[6] R D Hazeltine and J D Meiss, *'Plasma Confinement'* (Addison Wesley) 1992 p308
[7] J W Connor and J B Taylor, Phys Fluids **30** (1987) 3180
[8] Y Z Zhang and S M Mahajan, Phys Plasmas B**2** (1995) 4236
[9] J B Taylor and H R Wilson, Plas Phys Contr Fusion **38** (1996) 1999
[10] R L Miller, F L Waelbroeck, A B Hassam and R E Waltz, Phys Plasmas **2** (1995) 3676
[11] P Breger et al, Plas Phys Contr Fusion **40** (1998) 347